ADVANCED ENGINEERING MATERIALS

DOI: 10.1002/adem.201500179

Oxidation Behavior of $Al_8Co_{17}Cr_{17}Cu_8Fe_{17}Ni_{33}$, $Al_{23}Co_{15}Cr_{23}Cu_8Fe_{15}Ni_{15}$, and $Al_{17}Co_{17}Cr_{17}Cu_{17}Fe_{17}Ni_{17}$ Compositionally Complex Alloys (High-Entropy Alloys) at Elevated Temperatures in Air**

By *Haneen M. Daoud, Anna M. Manzoni, Rainer Völkl, Nelia Wanderka* and *Uwe Glatzel**

Oxidation behavior of the compositionally complex alloys (high-entropy alloys) $Al_8Co_{17}Cr_{17}Cu_8Fe_{17}Ni_{33}$ (fcc-alloy), $Al_{23}Co_{15}Cr_{23}Cu_8Fe_{15}Ni_{15}$ (bcc-alloy), and $Al_{17}Co_{17}Cr_{17}Cu_{17}Fe_{17}Ni_{17}$ (reference-alloy) at elevated temperatures in air is investigated. The microstructures of the oxide scales and the substrates are analyzed using scanning electron microscopy and X-ray diffraction. All oxidized alloys follow a parabolic kinetic law with low mass change per surface area at 800 °C. The $Al_8Cr_{17}Co_{17}Cu_8Fe_{17}Ni_{33}$ alloy follows sub-parabolic kinetic law at 1 000 °C and exhibits good oxidation resistance at both tested temperatures (800 and 1 000 °C). Two alloys, $Al_{23}Co_{15}Cr_{23}Cu_8Fe_{15}Ni_{15}$ and $Al_{17}Co_{17}Cr_{17}Cu_{17}Fe_{17}Ni_{17}$ suffer from strong spallation at 1 000 °C.

1. Introduction

Compositionally complex alloys have been named in the literature as high-entropy alloys.[1] We prefer the name compositionally complex alloys, since in most cases the so-called high-entropy alloys form one or more of ordered phases which leads to relatively low entropy. They can be defined as alloys containing five or more metallic elements with the concentration of each element varying in between 5 and 35 at.%.[1] The microstructures and mechanical behavior of these alloys are widely investigated.[2–6] The literature on compositionally complex alloys (high-entropy alloys) often reports promising properties such as high corrosion resistance,[7,8] high strength, and high hardness[6] at elevated temperatures which would enable their use in various applications for example as furnace parts, molds, and tools.[9,10] Good oxidation resistance is another key property in high-temperature applications. However, the oxidation behavior of compositionally complex alloys (high-entropy alloys) has rarely been investigated.[11,12] Kai *et al*.[11] investigated the oxidation behavior in air of the equimolar alloys $Co_{20}Cr_{20}Cu_{20}Fe_{20}Ni_{20}$, $Co_{25}Cr_{25}Fe_{25}Ni_{25}$, and $Co_{33}Fe_{33}Ni_{33}$ at temperatures between 800–1 000 °C. It was reported that the oxidation resistance of $Co_{33}Fe_{33}Ni_{33}$ alloy can be enhanced by adding Cr and Cu in both oxidized quaternary and quinary alloys.[11] The oxidation behavior of several refractory compositionally complex alloys (high-entropy alloys) in air at 1 300 °C has been investigated by Liu *et al*.[12] All the investigated alloys in the later work at the mentioned oxidation temperature followed linear kinetics.[12]

However, the oxidation behavior of the well-known $Al_{17}Co_{17}Cr_{17}Cu_{17}Fe_{17}Ni_{17}$ alloy has not been studied so far, although the microstructure of the as-cast alloy is widely investigated.[9,13] This equiatomic alloy consists of at least five phases.[13] In order to reduce the number of phases, the equiatomic composition of the alloy was modified in which two further alloys have been developed with two main phases as has been described recently.[14–16] One alloy forms an fcc structure ($Al_8Co_{17}Cr_{17}Cu_8Fe_{17}Ni_{33}$) and the other one a bcc structure ($Al_{23}Co_{15}Cr_{23}Cu_8Fe_{15}Ni_{15}$). The microstructure and the mechanical properties of these alloys have also been intensively analyzed.[14–16]

The focus of this work is, therefore, investigation of the high-temperature oxidation behavior of the compositionally complex alloys $Al_8Co_{17}Cr_{17}Cu_8Fe_{17}Ni_{33}$ (named fcc-alloy),

[*] *Dr. H. M. Daoud, Dr. R. Völkl, Prof. U. Glatzel*
Metals and alloys, Bayreuth University, Ludwig-Thoma Street. 36b, 95447 Bayreuth, Germany
E-mail: uwe.glatzel@uni-bayreuth.de
Dr. A. M. Manzoni, Dr. N. Wanderka
Helmholtz-Zentrum Berlin für Materialien und Energie GmbH, Hahn-Meitner-Platz 1, 14109 Berlin, Germany

[**] *The authors are grateful to the German Research Foundation (DFG) for the financial support by Grants GL 181/25-1 and WA 1378/15-1. The authors would like to thank Dipl.-Ing. S. Scheler (Ceramic Materials Engineering, Bayreuth University, Germany) for his help in the dilatometer measurements. Supporting Information is available from the Wiley Online Library or from the author.*

$Al_{23}Co_{15}Cr_{23}Cu_8Fe_{15}Ni_{15}$ (named bcc-alloy), and $Al_{17}Co_{17}Cr_{17}Cu_{17}Fe_{17}Ni_{17}$ (named reference-alloy). In which, the main aim of this work is to study the role of Al and Cr beside other elements in the oxidation behavior and the oxide scale formation.

2. Experimental Section

The investigated alloys are $Al_8Co_{17}Cr_{17}Cu_8Fe_{17}Ni_{33}$, $Al_{23}Co_{15}Cr_{23}Cu_8Fe_{15}Ni_{15}$, and $Al_{17}Co_{17}Cr_{17}Cu_{17}Fe_{17}Ni_{17}$ (in at.%). The alloys were prepared from 99.99% pure elements by vacuum induction melting and pouring into a cold Cu-mold (geometry: $100 \times 30 \times 14\,mm^3$). The dimensions of the specimens for oxidation experiments are $28.5 \times 12.0 \times 1.0\,mm^3$ and all the specimens have been oxidized in the as-cast state. The specimens for the oxidation tests of the $Al_8Co_{17}Cr_{17}Cu_8Fe_{17}Ni_{33}$ alloy were cut by a precision wafering saw (Buehler, Isomet 4000). Specimens of the more brittle $Al_{23}Co_{15}Cr_{23}Cu_8Fe_{15}Ni_{15}$ and the $Al_{17}Co_{17}Cr_{17}Cu_{17}Fe_{17}Ni_{17}$ alloys were prepared by wire electrical discharge machining (WEDM). The specimens were grinded using abrasive SiC papers (down to 1 200 grit) before oxidation. For oxidation tests, the specimens were put in a preheated furnace in air for different durations. After a defined time, the oxidized specimens were taken from the furnace and weighted after cooling down to room temperature, using a microbalance with an accuracy of ± 0.01 mg (Sartorius, BP112D). Oxidized specimens were embedded in non-conductive EpoFix (Struers A/S) cold mounting consumable.

After that, cross-sections of the samples were mechanically grinded and polished, lightly etched, and coated with gold for the analysis of the microstructures with a scanning electron microscope, SEM (Zeiss 1540 EsB crossbeam) equipped with an energy dispersive X-ray spectrometer (EDX). The EDX results are not shown here. Thin foil specimens for transmission electron microscopy (Philips, CM30) studies were thinned mechanically down to a thickness of around 10 μm and then Ar-ion milled with a voltage of 5 kV and a current of 2.5 mA until electron transparent. Crystal structures of oxide phases in the scales were identified by X-ray diffraction, XRD (Seifert 3000P, monochromatic Cu-$K\alpha_1$). The thermal coefficient of expansion for the investigated alloys has been measured using a high-temperature dilatometer (Netzsch, 402E/7) in Ar-environment with a heating rate of 10 °C min^{-1}. Cylindrical specimens of 9.0 mm in length for the fcc- and the bcc-alloys and 5.4 mm length for the reference-alloy.

3. Results

3.1. Microstructure of the Investigated Alloys

3.1.1. Fcc-Alloy ($Al_8Co_{17}Cr_{17}Cu_8Fe_{17}Ni_{33}$)

The microstructure of the fcc-alloy consists of an fcc solid solution matrix and precipitates with $L1_2$ structure. The precipitates are rich in Ni and Al and their mean diameter is below 20 nm with less than 20% volume fraction.[14,15] A previous study[15] also reported Ni-Al-Cu precipitates at grain boundaries with a volume fraction of less than 1% (Figure 1).

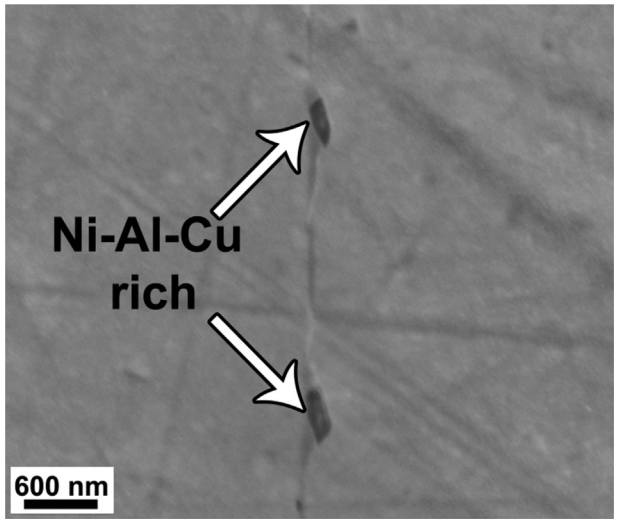

Fig. 1. SEM micrograph of the fcc-alloy shows Ni–Al–Cu-rich precipitates at a grain boundary.

3.1.2. Bcc-Alloy ($Al_{23}Co_{15}Cr_{23}Cu_8Fe_{15}Ni_{15}$)

The microstructure of the bcc-alloy (see Figure 2a–b) reveals a B2-ordered bcc matrix rich in Al and Ni with about 46% volume fraction. It is interesting to note that the majority phase is an intermetallic phase. Cuboidal and rectangular-shaped particles of a Cr- and Fe-rich bcc phase with about 43% volume fraction are embedded into the matrix and at the grain boundaries.[14] Tiny Cu-rich particles with fcc crystal structure constituting a third phase are found at the grain boundaries and inside the grains.[14]

3.1.3. Reference-Alloy ($Al_{17}Co_{17}Cr_{17}Cu_{17}Fe_{17}Ni_{17}$)

The reference-alloy solidifies into two zones named 1 and 2, which can be seen in Figure 2c-d. Zone 1 consists of an Al–Ni-rich B2-ordered bcc phase as matrix, in which platelets of a bcc phase enriched in Cr and Fe can be found.[13] In addition small Cu-rich precipitates with fcc structure can be seen. Zone 2 forms islands inside zone 1 and consists of a Cu-rich fcc phase[13] and Cr–Fe-rich precipitates with bcc structure. This bcc phase was not observed by our previous work.[13] Table 1 summarizes the microstructures of the three alloys.

3.2. Kinetics of Oxidation

The kinetics of the oxidation has been measured by the mass change per unit surface area after defined time intervals. The general oxidation law relationship (1) was used according to refs.[17–19];

$$\left(\frac{\Delta m}{A}\right)^n = kt \tag{1}$$

where Δm is the mass change, A is the surface area, k a kinetic constant, t is the exposure time, and n an exponential index.

DOI: 10.1002/adem.201500179

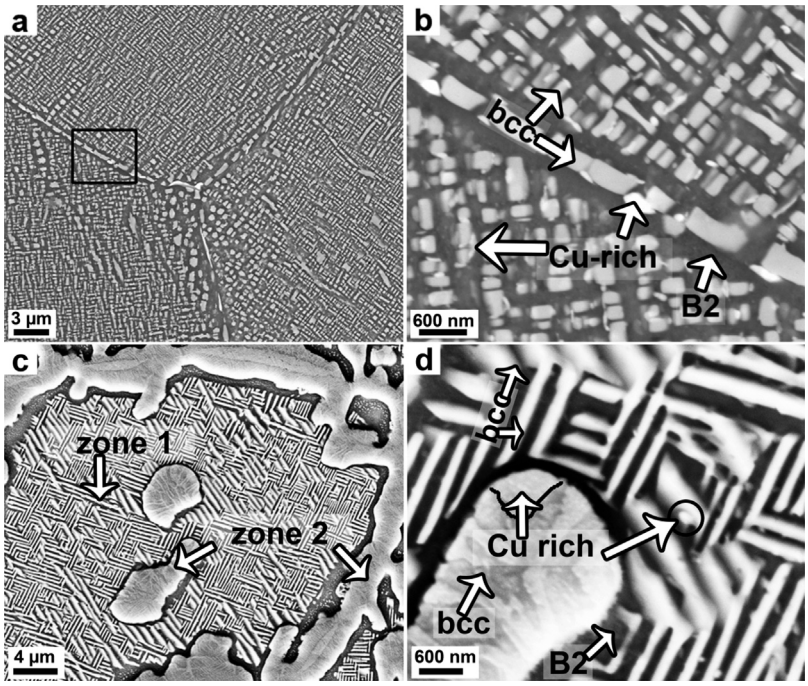

Fig. 2. SEM micrographs of the microstructure of (a–b) the bcc-alloy with grain boundaries and (c–d) the reference-alloy, (a and c) at low magnification and (b and d) at high magnification.[16]

3.2.1. Kinetics of Oxidation at 800 °C

The mass change per surface area versus time at 800 °C is plotted in Figure 3a. A small mass loss trend has been noticed for all the oxidized alloys at 800 °C (see Figure 3). This could be attributed to many possible effects like possible spallation or weighting error of the several oxidized specimens. However, the measured value of n (see equation 1) for all three investigated is 2. The general trend can be attributed to a parabolic growth law. The value of the parabolic constants for both the fcc- and the bcc-alloys at 800 °C is $3 \cdot 10^{-2}\,g^2\,m^{-4}\,h^{-1}$ and for the reference-alloy $4 \cdot 10^{-2}\,g^2\,m^{-4}\,h^{-1}$. These values indicate that the oxidation rate of the investigated alloys is relatively low and close to each other.

Table 1. Comparison of the phases obtained in the fcc-, bcc-, and reference-alloys.

Alloy	XRD, SEM/EDX, TEM/EDX	Volume fraction [%]	Size [nm]
Fcc-alloy[14,15]	Matrix: fcc solid solution	rest	–
	Al–Ni-rich γ′ precipitates	<20	<20
	Ni–Al–Cu-rich precipitates at grain boundaries	$<0.7 \pm 0.6$	100 – 450
Bcc-alloy[14]	Matrix: Al–Ni-rich, B2	46	–
	Cr–Fe-rich bcc precipitates	43	100 – 1 000
	Cu-rich fcc precipitates	6	50 – 400
Reference-alloy[13]	Zone 1:		
	Matrix: Al–Ni-rich, B2	–	–
	Plate-like Cr–Fe precipitates, bcc	–	–
	Cu-rich fcc precipitates	–	–
	Zone 2:	–	–
	Cr–Fe-rich precipitates, bcc (this work)	–	–
	Cu-rich fcc matrix	–	–

3.2.2. Kinetics of Oxidation at 1 000 °C

Figure 3b shows the mass change per surface area versus time at 1 000 °C. The oxidation at this temperature shows an increase of the mass change for the fcc-alloy unlike the bcc- and reference-alloys. However, also at this temperature as at 800 °C, a mass loss trend has been observed and it is small in case of the oxidized fcc-alloy and huge in both of the oxidized bcc- and reference-alloys (see Figure 3b). Therefore, the precise determination of kinetics is not possible in case of the bcc- and the reference-alloys. The fcc-alloy has the measured value of n equal to 5, which indicates that the alloy follows a sub-parabolic law.

As reported above, the mass change curves for both the bcc- and the reference-alloys show a strong decrease in the mass change (see Figure 3b) due to spallation of oxide layers. This happened every time when the oxidized specimens are taken out from the furnace and cooled down to room temperature, indicating a poor adhesive behavior and/or strong difference in the thermal expansion coefficients.

Figure 4 illustrates the spallation effect of oxide scales by showing a rest of the oxide layers on the surfaces of the bcc- and reference-alloys after cooling down the specimens from 1 000 °C/200 h to room temperature. In the case of the oxidized reference-alloy specimen, only a thin oxide layer is still visible on its surface, as can be noticed from the bright color of the oxide layer (see Figure 4). The same effect of spallation can be seen in the oxidized bcc-alloy specimen. Here the substrate layer can be seen in some places where no oxide layers are left (Figure 4). However, thick and continuous oxide layers form on the surface of the fcc-alloy and it does not show huge spallation like the oxidized bcc- and fcc-alloys (Figure 4).

3.3. Characterization of Oxide Layers at 800 °C

3.3.1. Scale Morphology of the Oxidized Fcc-Alloy

After oxidation at 800 °C in air, the fcc-alloy shows the formation of a rough oxide layer, see Figure 5a. The scale consists of three layers. The investigation of the elemental distribution (not shown here) indicates that the outer layer

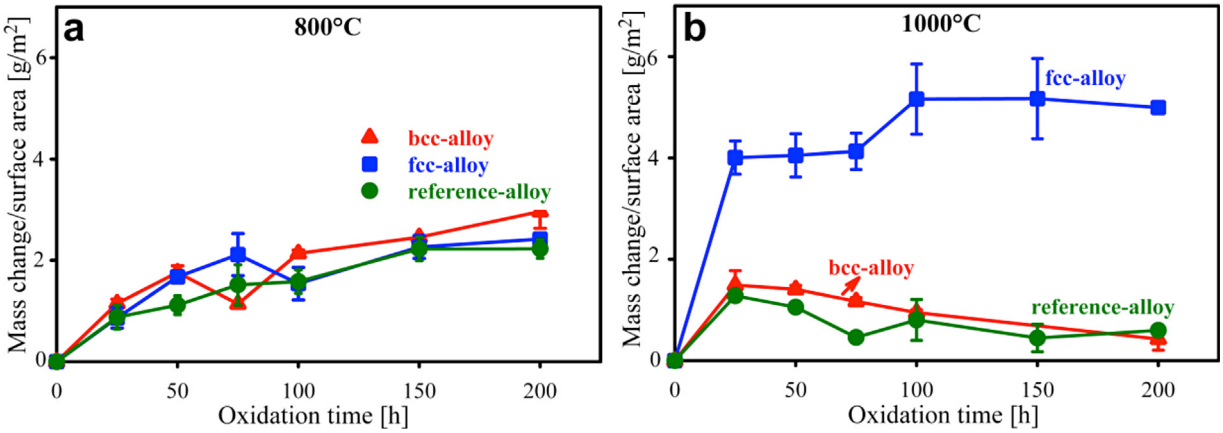

Fig. 3. The mass change per surface area versus time curves (a) at 800 °C and (b) at 1 000 °C for the fcc-, bcc-, and reference-alloys.

consists mainly of Ni and Fe oxides. Chromium oxide forms an intermediate layer and aluminum oxide the innermost oxide layer. The thickness of the scale is 6.5 ± 2.4 μm. It should be noted that below the oxides at the interface to the substrate, a layer of about 5.0 ± 1.4 μm depleted in aluminum is formed. Kirkendall voids marked by an arrow are also visible in the Al-depleted region.

The crystal structures of the oxides are analyzed by XRD. Figure 6a shows XRD patterns related to NiO, Cr_2O_3, Al_2O_3, and Fe oxides. The formation of Fe_2O_3 and Fe_3O_4 oxides is possible. However, it is difficult to decide which one is present in the oxide scale because the diffraction peaks of both oxide types appear at almost the same positions in the spectra, as already noted by Kai *et al.*[11]

3.3.2. Scale Morphology of the Oxidized Bcc-Alloy

Figure 5b shows that the bcc-alloy forms a single oxide layer with a thickness of 2.1 ± 0.2 μm after 800 °C/200 h in air. The XRD measurements (Figure 6b) confirm that the scale consists mainly of aluminum oxide. In the substrate, close to the oxide layer, again a 4.0 ± 1.8 μm thick Al-depleted zone is observed. The zone has an irregular shape and is rich in Cr and Fe. Cu-rich precipitates are found at the transition area from the depletion zone to the alloy interior (see Supporting Information).

Additional peaks referred to σ-phase are identified in the XRD pattern of the oxidized bcc-alloy specimen (see Figure 6b). A TEM-bright field micrograph (see Supporting Information) of the depletion zone reveals a fine particle containing Cr, Fe, and Co (composition shown in the Supporting Information). The diffraction pattern corresponds to a [1–40] zone axis

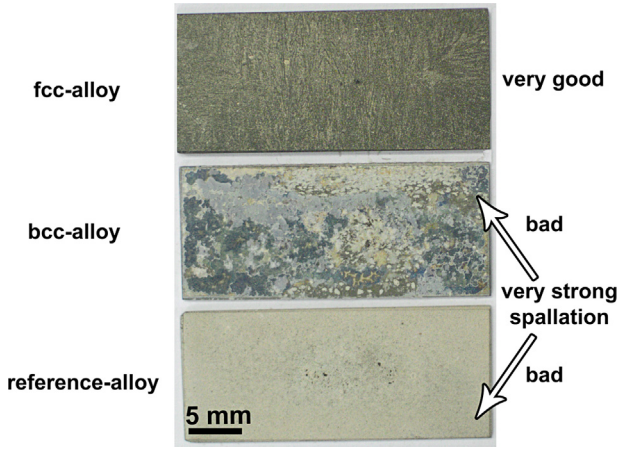

Fig. 4. Optical micrograph of the specimens oxidized at 1 000 °C/200 h. The oxide layers in the case of the bcc- and reference-alloys spall off and the surfaces are covered discontinuously with a thin layer. Thick oxide layers form and cover the entire specimen of the fcc-alloy.

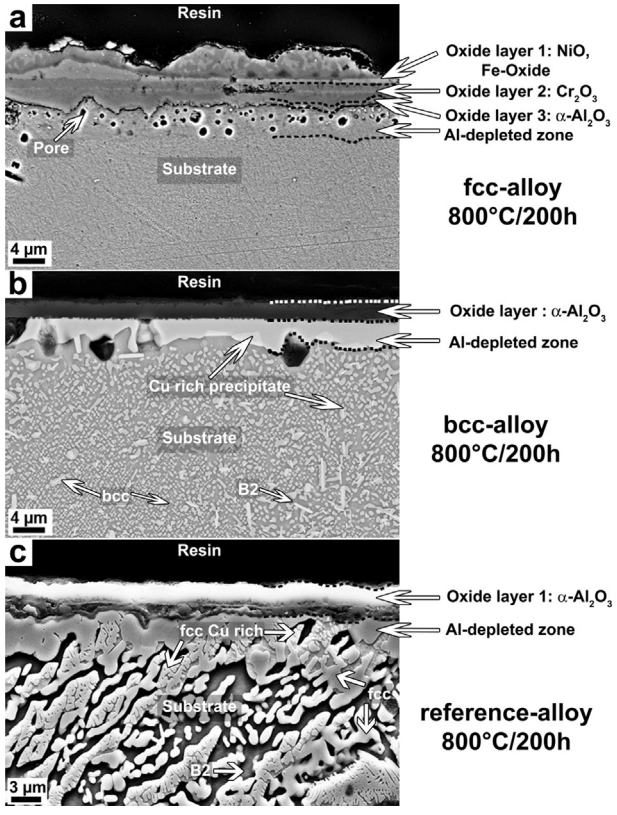

Fig. 5. SEM-micrographs of the cross-sectioned specimens of the (a) fcc-alloy, (b) bcc-alloy, and (c) reference-alloy oxidized at 800 °C/200 h (bcc phase is rich in Cr and Fe and B2 phase in Al and Ni).

DOI: 10.1002/adem.201500179

ADVANCED ENGINEERING MATERIALS

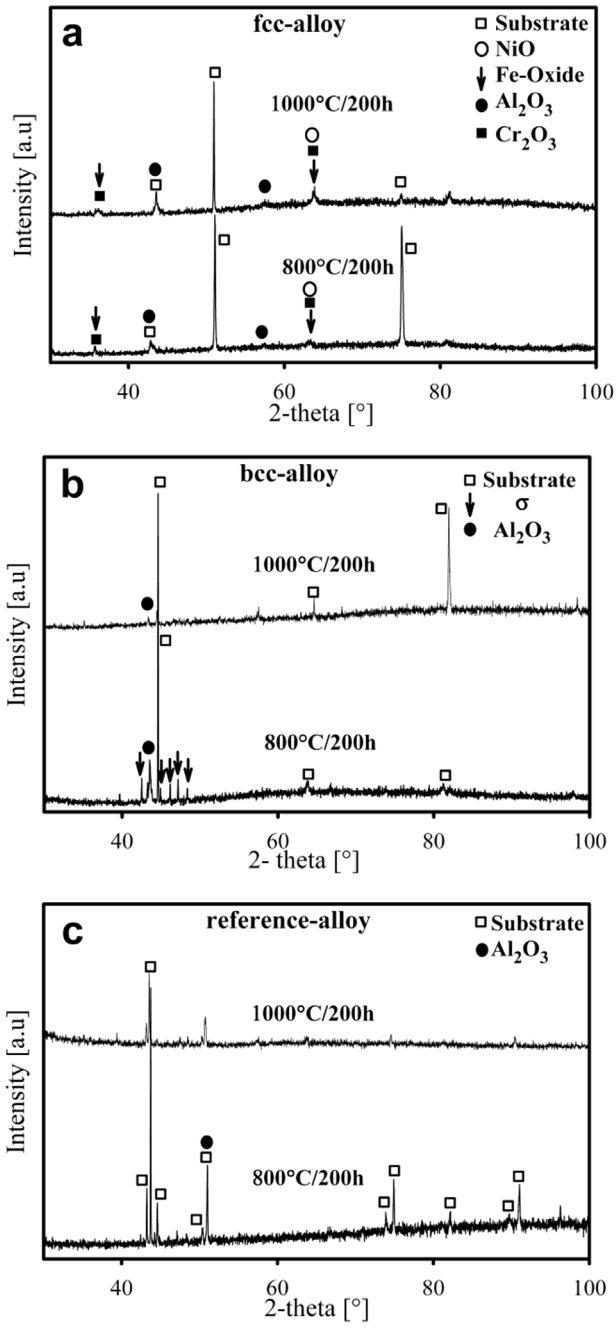

Fig. 6. XRD patterns of (a) the fcc-alloy oxidized, (b) bcc-alloy, and (c) reference-alloy at 800 °C/200 h and 1 000 °C/200 h.

pattern of a tetragonal σ-phase with lattice parameters $a = 898.1$ pm and $c = 469.0$ pm. The TEM-SAD results are in good agreement with the XRD-measured lattice parameters of $a = 880.0$ pm and $c = 454.4$ pm for this tetragonal phase (see Figure 6b and the Supporting Information).

The simulated phase diagram of the bcc-alloy using the Thermo-Calc software and the TTNi7 database confirms the presence of a σ-phase at intermediate temperatures between 525 and 750 °C.[14,16] The calculated composition (in at.%) of this phase is $Cr_{54}Fe_{32}Co_{13}Ni_1$ at 800 °C (see the Supporting Information).

3.3.3. Scale Morphology of the Oxidized Reference-Alloy

The reference-alloy also forms an α-Al_2O_3 scale close to an Al-depleted zone (see Figure 5c) during exposure to air at 800 °C. The XRD pattern of the oxidized reference-alloy is shown in Figure 6c.

3.4. Characterization of the Oxide Layers at 1 000 °C

3.4.1. Scale Morphology of the Oxidized Fcc-Alloy

The scale morphology and the XRD pattern of the oxidized fcc-alloy at 1 000 °C/200 h are shown in Figure 7a and 6a, respectively. The scale continues to have multi-oxide layers in a similar way as at 800 °C. Al-oxide forms in the inner oxide layer, Cr-oxide in the outer layer. The thickness of the scale is 6.3 ± 3.0 μm. The XRD pattern confirms that formed oxides are Al_2O_3 and Cr_2O_3 (see Figure 6a).

3.4.2. Scale Morphology of the Oxidized Bcc- and Reference-Alloys

Both the bcc- and the reference-alloys suffer huge spallation after oxidation at 1 000 °C during the cooling process. The previously shown micrograph of the oxidized specimens at 1 000 °C/200 h (see Figure 4) indicates that the formed oxides on both surfaces of the bcc- and the reference-alloys are discontinuous and do not cover the whole specimens, since they spall off during cooling.

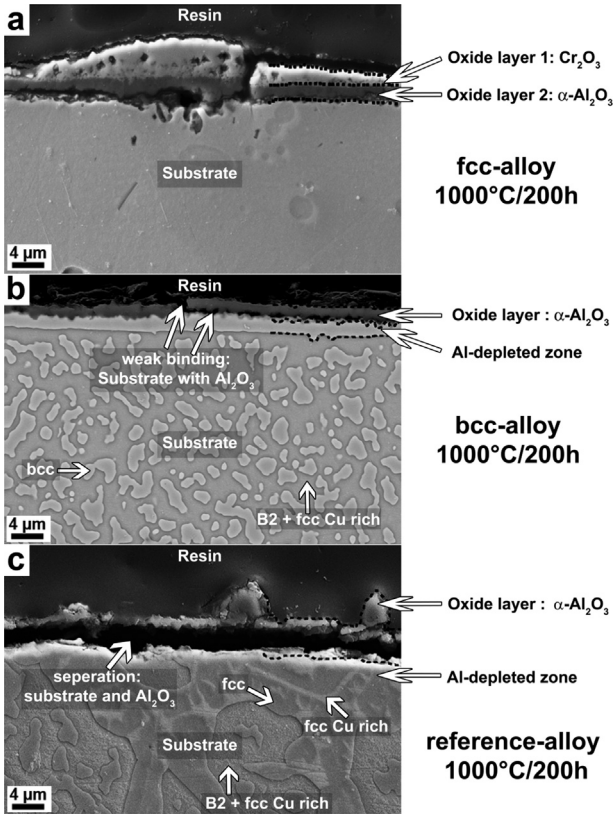

Fig. 7. SEM-micrograph of the cross-sectioned specimen of the (a) fcc-alloy, (b) bcc-alloy, and (c) reference-alloy oxidized at 1 000 °C/200 h (bcc phase is rich in Cr and Fe and B2 phase in Al and Ni).

DOI: 10.1002/adem.201500179

Table 2. Comparison of the oxide layers in the scale of the three oxidized alloys at 800 °C and 1000 °C after 200 h.

	800 °C/200 h		1 000 °C/200 h	
Alloy	Oxides	Thickness [μm]	Oxides	Thickness [μm]
Bcc	Fe oxide, NiO/ Cr_2O_3/ Al_2O_3	6.5 ± 2.4	Cr_2O_3, Al_2O_3	6.3 ± 3.0
Fcc	Al_2O_3	2.1 ± 0.2	Al_2O_3	–
Reference	Al_2O_3	3.4 ± 0.9	Al_2O_3	–

The scale morphologies of the bcc- and reference-alloys are shown in Figures 7b and c, respectively. Figure 6b and c represent the XRD patterns for the oxidized surface of the bcc- and reference-alloys, respectively. In both cases, an Al-depleted zone forms below an alumina layer. Furthermore, the SEM micrographs show cracks in between the alumina layer and the substrate, as can be seen in Figure 7b and c. For further information about the microstructural evolution of the substrate after oxidation, we recommend ref.[16]

Table 2 summarizes the compositions and the thicknesses of the formed scales in the alloys oxidized at 800 °C/200 h and 1 000 °C/200 h.

4. Discussion

Our results show that the oxidation behavior depends on temperature and composition of the investigated alloys. The temperature influences the diffusion of the species, which controls the oxidation rate.[17–19] It also influences the oxidation kinetics. The oxidation kinetics convert from parabolic law ($\Delta m/A = t^{1/2}$) at 800 °C to sub-parabolic ($\Delta m/A = t^{1/5}$) at 1 000 °C in the case of the fcc-alloy, which provides more protection against oxidation. In comparison to parabolic kinetic law ($\Delta m/A = t^{1/2}$), the mass gain at the beginning of oxidation according to the sub-parabolic law increases faster and after that it slows down ($\Delta m/A = t^{1/5}$) which is in accordance with ref.[21] However, for bcc- and reference-alloys, it was not possible to determine the oxidation kinetics because of spallation that occurs during the cooling process.

The protective layers α-alumina (and chromia) formed in the scale of the three oxidized alloys at 800 °C promote the oxidation resistance. As reported previously, the alumina and chromia are considered to be good protective oxide layers against oxidation.[18,19] The most important properties for a scale to be a protective layer against oxidation are as follows: high-thermal stability, good adherence, and continuous and slow growth. Both alumina and chromia have high melting points and high negative formation energy. In addition to that alumina grows very slowly due to its complex corundum structure.[18,22]

Two main factors control the formation of continuous alumina: the oxidation temperature and sufficient mole fraction of Al in the alloy. The formation of alumina is enhanced by an increase in oxidation temperature. The observed alumina is three times thicker at 1 000 °C than at 800 °C after the same oxidation time (see Figure 5a and 7a). The high mole fraction of Al in both the bcc- and the reference-alloys enables the formation of only alumina and inhibits the formation of any other oxides. This effect is well known for alumina-forming alloys which contain high mole fractions of Al.[19,22,23] This single alumina layer does not provide protection against oxidation, possibly due to the great susceptibility of alumina to spallation. The great susceptibility to spallation could be explained by the large difference between the thermal coefficients of expansion of the alumina and the substrate.[19,22,24] This large difference of the thermal coefficients of expansion leads to high stress levels within substrate and oxide scale. This stress facilitates the scale to spall during the cooling from the oxidation temperature. Stresses can be approximated by Equation 2:[24]

$$\sigma = \frac{-(\alpha_{Ox} - \alpha_M)\Delta T}{\frac{2t_{Ox}(1-v_M)}{t_M E_M} + \frac{(1-v_{Ox})}{E_{Ox}}} \quad (2)$$

where, σ is the compressive stress of the oxide, ΔT the difference between the oxidation temperature and cooling temperature, a_M and α_{Ox} are the thermal coefficients of expansion of the metal and its oxide, respectively, E_M and E_{Ox} are the elastic moduli of the metal and the oxide, respectively, and v_M and v_{Ox} are Poisson ratios of the metal and oxides, respectively. Table 3 shows the values of the thermal coefficients of expansion of the mentioned oxides and the investigated alloys in this work. There is a large difference between the thermal coefficient of the expansion of alumina and the oxidized alloys.

In order to promote the adherence of alumina, other elements can be added. This is known as the third element effect.[19] It is well known that chromium acts as a getter for Al by providing sites for reaction with oxygen ions according to the following reaction (3):[19]

$$Cr_2O_3 + 2Al \rightarrow Al_2O_3 + 2Cr \quad (3)$$

As reported in refs.,[19,21,22] adding Cr to the composition reduces the required mole fraction of Al to form a stable

Table 3. Thermal coefficients of expansion of some oxides[19] and investigated alloys.

Metal-oxide system	Thermal coefficient of expansion (α) $10^{-6}[K^{-1}]$	Temperature range [K]
Fe_2O_3	14.9	290 – 1 200
NiO	17.1	290 – 1 273
Cr_2O_3	7.3	100 – 1 273
Al_2O_3	5.1–9.8	298 – 1 438
Fcc-alloy	20.4	573 – 1 600
Bcc-alloy	23.0	573 – 1 480
Reference-alloy	25.7	573 – 1 381

DOI: 10.1002/adem.201500179

Table 4. Comparison between the oxidation behavior of the three oxidized alloys with two commercial alloys (Inconel 617 and Alloy 800).

	Oxidation test [air, 100 h]		Composition [wt.%]	
Alloy	Weight change [g m^{-2}]	Temperature [°C]	Al	Cr
Fcc-alloy	2	800	4	16
	5	1 000		
Bcc-alloy	2	800	12	24
	Spallation	1 000		
Reference-alloy	5	800	8	16
	Spallation	1 000		
Inconel 617[25]	5	900	1.1	22
	≈−3.4	1 100		
Alloy 800[26]	8	927	0.4	21
	21	1 038		

external alumina layer. Indeed the stable oxide scale has been observed in the alloy with the smallest mole fraction of Al. The fcc-alloy stands out not only by a low Al content but also by a Cr/Al ratio of 2 which is twice as high as in the bcc- and the reference-alloys. This ratio may be a contributing factor for the stabilization of passive oxide layers. In the case of this ratio, the oxide layers remain on the substrate, whereas in the case of a 1:1 ratio as in bcc- and reference-alloys the scale spalls off. It can be concluded that the mole fraction of Cr und Al and other elements in the chemical compositions of an alloy should be optimized to provide better protection against oxidation. Another possibility to improve the scale plasticity of alumina in case of bcc- and reference-alloys could be the addition of other reactive elements like Y.[22]

Table 4 represents a comparison between the oxidation behavior in air of the three oxidized alloys with two other commercial alloys: Inconel 617 and Alloy 800. Both of the mentioned commercial alloys exhibit a good oxidation resistance and, therefore, they are used often as high-temperature gas-cooled reactors and heat-resistant plates at elevated temperatures, respectively.[25,26] The fcc-alloy exhibits better oxidation resistance than the two last mentioned alloys. This could be attributed to that fact that the fcc-alloy forms both of protected Cr and Al-oxides, where both of Alloy 800 and Inconel 617 form principally Cr-oxide.[25,26] In addition to Cr-oxide, Inconel 617 forms a thin layer from Al-oxide (see in Table 4 the weight percents of Al and Cr in the compositions of the three oxidized alloys comparing to Inconel 617 and Alloy 800).

5. Summary

High-temperature oxidation of $Al_8Co_{17}Cr_{17}Cu_8Fe_{17}Ni_{33}$ (fcc-alloy), $Al_{23}Co_{15}Cr_{23}Cu_8Fe_{15}Ni_{15}$ (bcc-alloy), and $Al_{17}Co_{17}Cr_{17}Cu_{17}Fe_{17}Ni_{17}$ (reference-alloy) alloys at 800 °C/200 h and 1 000 °C/200 h in air has been investigated. At 800 °C, all three alloys show low mass change up to 200 h following parabolic kinetics. The scale of the fcc-alloy consists of three layers, alumina as the inner scale, chromia layer above it, and both iron oxide and nickel oxide at the outer layer. The scales of the bcc- and the reference-alloys consist of alumina oxide only.

At 1 000 °C, the fcc-alloy shows a higher mass change and the kinetics follows sub-parabolic law. The scale forms double oxide layers of alumina and chromia. The bcc- and reference-alloys suffer strong spallation and only alumina has been detected on the surfaces of both oxidized alloys. The ratio Cr/Al, twice as high in the fcc-alloy as in the bcc- and the reference-alloys, might have an influence on this oxidation behavior.

Received: April 1, 2015
Final Version: May 26, 2015

[1] J. W. Yeh, S. K. Chen, S. J. Lin, J. Y. Gan, T. S. Chin, T. T. Shun, C. H. Tsau, S. Y. Chang, *Adv. Eng. Mater.* **2004**, *6*, 299.
[2] A. Manzoni, H. Daoud, R. Völkl, U. Glatzel, N. Wanderka, *Ultramicroscopy* **2013**, *132*, 212.
[3] K. B. Zhang, Z. Y. Fu, J. Y. Zhang, J. Shi, W. M. Wang, H. Wang, Y. C. Wang, Q. J. Zhang, *J. Alloys. Compd.* **2010**, *502*, 295.
[4] M. H. Tsai, H. Yuan, G. Cheng, W. Xu, K. Y. Tsai, C. W. Tsai, W. W. Jian, C. C. Juan, W. J. Shen, M. H. Chuang, J. W. Yeh, Y. T. Zhu, *Intermetallics* **2013**, *32*, 329.
[5] A. V. Kuznetsov, D. G. Shaysultnov, N. D. Stepanov, G. A. Salishchev, O. N. Senkov, *Mater. Sci. Eng. A* **2012**, *533*, 107.
[6] O. N. Senkov, G. B. Wilks, J. M. Scott, D. B. Miracle, *Intermetallics* **2011**, *19*, 698.
[7] Y. Y. Chen, T. Duval, U. D. Hung, J. W. Yeh, H. C. Shih, *Corros. Sci.* **2005**, *47*, 2257.
[8] X.-W. Qiu, Y.-P. Zhang, L. He, C.-G. Liu, *J. Alloys. Compd.* **2013**, *549*, 195.
[9] C. J. Tong, Y. L. Chen, S. K. Chen, J. W. Yeh, T. T. Shun, C. H. Tsau, S. J. Lin, S. Y. Chang, *Metall. Mater. Trans. A* **2005**, *36*, 881.
[10] C. C. Tung, J. W. Yeh, T. T. Shun, S. K. Chen, Y. S. Huang, H. C. Chen, *Mater. Lett.* **2007**, *6*, 1.
[11] W. Kai, W. L. Jang, R. T. Huang, C. C. Lee, H. H. Hsieh, C. F. Du, *Oxid. Met.* **2005**, *63*, 169.
[12] C. M. Liu, H. M. Wang, S. Q. Zhang, H. B. Tang, A. L. Zhang, *J. Alloys. Compd.* **2014**, *583*, 162.
[13] S. Singh, N. Wanderka, B. S. Murty, U. Glatzel, J. Banhart, *Acta Mater.* **2011**, *59*, 182.
[14] A. Manzoni, H. Daoud, S. Mondal, S. van Smaalen, R. Völkl, U. Glatzel, N. Wanderka, *J. Alloys. Compd.* **2013**, *552*, 430.
[15] H. M. Daoud, A. Manzoni, R. Völkl, N. Wanderka, U. Glatzel, *JOM. J. Min. Met. Mat. S.* **2013**, *65*, 1805.
[16] H. M. Daoud, PhD Thesis, *Mikrostruktur, mechanische Eigenschaften und Oxidationsverhalten von Legierungen mit*

komplexer Zusammensetzung (Hochentropielegierungen), Shaker verlag, Aachen, Germany **2014**.
[17] A. S. Khanna, *Introduction to High Temperature Oxidation and Corrosion*, Materials Park, OH, United States of America **2002**, p. 53, 202.
[18] R. Davis, *Heat Resistant Materials*, ASM Specialty Handbook, Materials Park, OH, United States of America **1997**, p. 31.
[19] D. J. Young, *High Temperature Oxidation and Corrosion of Metals*, Oxford, United Kingdom **2008**, p. 71, 338.
[20] L. H. Wen, H. C. Kou, J. S. Li, H. Chang, X. Y. Xue, L. Zhou, *Intermetallics* **2009**, *17*, 266.
[21] R. Haugsrud, *Corros. Sci.* **2003**, *45*, 211.
[22] R. Prescott, M. J. Graham, *Oxid. Met.* **1992**, *38*, 233.
[23] V. K. Tolpygo, D. R. Clarke, *Mater. Sci. Eng. A* **2000**, *278*, 151.
[24] N. Birks, G. H. Meier, F. S. Pettit, *Introduction to the High-temperature Oxidation of Metals*, Cambridge University Press, Cambridge, United Kingdom **2006**, 2nd ed., p. 138.
[25] C. Jang, D. Lee, D. Kim, *Int. J. Pres. Ves. Pip.* **2008**, *85*, 368.
[26] Sandmeyer Steel Company website. http://www.sandmeyersteel.com/images/Alloy-800-Spec-Sheet.pdf (Accessed 26 May, 2015).

ADVANCED ENGINEERING MATERIALS **2015**,
DOI: 10.1002/adem.201500179